Construction and Building Materials 84 (2015) 354–366

Contents lists available at ScienceDirect

Construction and Building Materials

journal homepage: www.elsevier.com/locate/conbuildmat

Analytical and experimental flexural behavior of concrete beams reinforced with glass fiber reinforced polymers bars

Maher A. Adam, Mohamed Said, Ahmed A. Mahmoud, Ali S. Shanour *

Department of Civil Engineering, Faculty of Engineering, Benha University, 108 Shoubra St., Shoubra, Cairo, Egypt

HIGHLIGHTS

- Glass fiber reinforced polymers (GFRP) bars were produced in the lab.
- Ten half-scale concrete beams were tested to study flexural behavior.
- Crack widths, deflection, mode of failure and GFRP bar strains were discussed.
- Non-linear finite element analyses was performed and assessed with experimental results.
- Amendments to ACI 440-06 formula for predicting (I_e) were introduced.

ARTICLE INFO

Article history:
Received 24 December 2014
Received in revised form 2 March 2015
Accepted 8 March 2015

Keywords:
Concrete beams
Locally produced
GFRP bars
Deflection
Effective moment of inertia
NLFEA

ABSTRACT

This paper presents an experimental, numerical and analytical study of the flexural behavior of concrete beams reinforced with locally produced glass fiber reinforced polymers (GFRP) bars. Glass fiber reinforced polymers (GFRP) reinforcement bars has a lower stiffness than steel reinforcement, which should be accounted for the ultimate and serviceability conditions, including the impact on member deflection and crack widths. The bars are locally produced by double parts die mold using local resources raw materials. A total of ten beams, measuring 120 mm wide × 300 mm deep × 2800 mm long, were cast and tested up to failure under four-point bending. The main parameters were reinforcement material type (GFRP and steel), concrete compressive strength and reinforcement ratio (μ_b, 1.7 μ_b and 2.7 μ_b; where μ_b is the reinforcement ratio at balanced condition). The mid-span deflection, crack width and GFRP reinforcement strains of the tested beams were recorded and compared. The test results revealed that the crack widths and mid-span deflection were significantly decreased by increasing the reinforcement ratio. The ultimate load increased by 47% and 97% as the reinforcement ratio increased from μ_b to 2.7 μ_b. Specimens reinforced by 2.7 μ_b can produce some amount of ductility provided by the concrete. The recorded strain of GFRP reinforcement reached to 90% of the ultimate strains. A non-linear finite element analysis (NLFEA) was constructed to simulate the flexural behavior of tested beams, in terms of crack pattern and load deflection behavior. It can be considered a good agreement between the experimental and numerical results was achieved. Modifications to ACI 440.1R-06 equation for estimating the effective moment of inertia (I_e) of FRP-reinforced concrete beams, using regression analysis of experimental results, is proposed by introducing empirical factors that effectively decrease the I_e at high load level. The proposed equation is compared with different code provisions and previous models for predicting the deflection. It can proved that the proposed factors gives good estimation for the effective moment of inertia (I_e) works well for FRP-reinforced concrete beams at high load level.

© 2015 Elsevier Ltd. All rights reserved.

1. Introduction

Steel reinforcement corrodes rapidly under aggressive conditions such as marine environments. The corrosion is caused by chloride ions, which can be found in de-icing salts in northern climates and sea water along coastal areas. Other materials, such as Fiber Reinforced Polymers (FRP), have emerged as an alternative to steel reinforcement when the exposure situation of the RC member requires durability under aggressive conditions. FRP products are composite materials consisting of a matrix (resin) and reinforcing fibers. The fibers are stronger than the matrix. In order to provide the reinforcing function, the fiber-volume fraction should be more than 55 percent for FRP bars and rods [21]. FRP materials

* Corresponding author. Tel.: +20 111 077 40 51.
E-mail addresses: maher.adam@feng.bu.edu.eg (M.A. Adam), mohamed.abdelghaffar@feng.bu.edu.eg (M. Said), ahmed.m5882@gmail.com (A.A. Mahmoud), ali.shnor@feng.bu.edu.eg (A.S. Shanour).

http://dx.doi.org/10.1016/j.conbuildmat.2015.03.057
0950-0618/© 2015 Elsevier Ltd. All rights reserved.

are anisotropic and are characterized by high tensile strength with no yielding only in the direction of the reinforcing fibers. This anisotropic behavior of GFRP bars affects the shear strength and dowel action as well as their bond performance [23]. The most common types of fibers are carbon, glass, and aramid. Glass fiber reinforced polymers (GFRP) bars have linear stress–strain behavior under tension up to failure; however, they have lower modulus of elasticity and no ductility like the steel bars. Therefore FRP reinforcement is not recommended for moment resistance frames or zones where moment redistribution is required [25].

The flexural behavior of concrete members reinforced with glass fiber-reinforced polymer (GFRP) reinforcing bars experimentally investigated by a number of studies [13,26,19,27]. They accounted for variations in concrete strength f'_c, reinforcement ratio ρ, FRP bars type, and shear span-depth ratio (a_v/d). It was found that the ACI 440.1R model overestimate the effective moment of inertia. They proposed modifying Branson's original equation for the effective moment of inertia and introduced modification factors for FRP-RC members. Abdul Rahman and Narayan [1] analyzed the performance of the beams in terms of their load carrying capacity and found that beams reinforced with GFRP bars experienced 3 times larger deflection at the same load level compared with steel reinforced beam. In addition, Balendran et al. [12], concluded that the ultimate strength of sand coated GFRP reinforced specimens was 1.4–2.0 times greater than that of the mild steel reinforced specimens but exhibited a higher deflection. The design of FRP-reinforced concrete beams is usually governed by the serviceability limit state requirements (crack width and deflection criteria) rather than ultimate limit state requirements [22]. Consequently, a modified expression is needed to predict the expected service load deflections of FRP-reinforced members with a reasonably high degree of accuracy.

The aims of this paper are, firstly, to produce GFRP bars using the available raw material in the local market, secondly, to present results of an experimental study of concrete beams reinforced with locally produced GFRP bars in terms of the deflection behavior, cracking, and ultimate load carrying capacity. Three different amounts of GFRP reinforcement and three grades of concrete compressive strength were used for that purpose. Numerical models using nonlinear finite element analysis (NLFEA) were conducted to evaluate the beams behavior by ANSYS software. In addition, analytical models for predicting the deflection of FRP-reinforced concrete beams are compared with experimental results. This comparison showed a need for reliability analysis of FRP codes equations for calculating the deflection. Modified equation that correlates well with experimental results was introduced. Regression analysis is used in order to bridge the gap between the experimental results and the calculated values.

2. Test program

2.1. Glass FRP reinforcement bars manufacturing and testing

The test program is a part of an extensive research project that was carried out to study the behavior of concrete beams reinforced with GFRP bars [6]. The GFRP bars were manufactured by the authors using glass fiber roving and resin. Double sets of plastic mold were manufactured at private workshop to manufacture 2.80 m long GFRP bars with 12 mm diameter. The GFRP ribbed bar of 12 mm diameter and double sets of plastic mold are shown in Fig. 1. The cross-sectional area and equivalent diameter of the GFRP bars were determined using the test method B.1 from (ACI 440.3R-04) [3]. Tensile and modulus properties were determined according to ASTM Standard (ASTM D7205-06) [11]. Nine tension coupons were tested to determine the failure stress and modulus of elasticity. The tensile stress of GFRP bars was determined as the average tensile strength of the GFRP bar specimens of diameter 12 mm and was found to be 640 MPa.

2.2. Test specimens

Ten GFRP RC beams were designed as simple span, with an adequate amount of longitudinal and shear reinforcement to fail by either tensile failure by rupture of GFRP bars or crushing of concrete in the central zone. Additionally, one RC beam with similar amount of steel reinforcement to one type of the GFRP RC elements was tested as a control beam for comparison purposes. Two 8 mm GFRP rebar were used as top reinforcement to hold stirrups. Three different amounts of longitudinal reinforcement ratios (μ_b, 1.7 μ_b and 2.7 μ_b; where μ_b is the reinforcement ratio at balanced condition based on Eq. (5–3) [18], and three different concrete grades (25, 45, and 70 MPa) were used. Standard compressive-strength tests of twelve concrete cubes (158 mm × 158 mm × 158 mm) were performed using a MTS-200 testing machine for each concrete grade respectively. The steel reinforced concrete beam was designed to behave with the same cracked stiffness as the GFRP RC element with concrete compressive strength of 25 MPa and reinforced with ratio of 2.7 μb. The beam tests layout is detailed in Fig. 2.

Details of the tested beams are summarized in Table 1. The beam types were identified as A-yy-z. The first term of the identification corresponded to a beams group. The second parameter identifies the beam series, characters 25 denoted that a target concrete strength of the series is 25 MPa, whilst 45 and 70 denoted that a target concrete strength of the series is 45 MPa and 70 MPa respectively. The last term indicates the specimen reinforcement, identification 1 for reinforcement ratio equal μ_b, identification 2 for reinforcement ratio equal 1.7 μ_b, and identification 3 for reinforcement ratio equal 2.7 μ_b.

2.3. Test setup

The specimens were tested under four-point bending, with 2500 mm effective span, and 1100 mm shear span, the distance between loads being 300 mm. Each specimen was supported on roller assemblies and knife edges to allow longitudinal motion and rotation. Fig. 3 shows the test setup and instrumentations for tested specimen. Two linear variable differential transformers (LVDT) were installed horizontally at the center of the specimen in the constant moment region to measure the neutral axis depth. Electrical resistance strain gauges were applied to the GFRP bars to measure the strain during the tests. The strain gages, electrical pressure sensors, and (LVDTs) voltages were fed into the data acquisition system. Each specimen was loaded in 30–70 increments. The cracks of the specimens were mapped and test observations were recorded during loading and at the time of failure. Fig. 4 shows the crack growth of specimen A25-3.

3. Test results and discussion

During the test, the beams were observed visually until the first crack appeared and the corresponding load was recorded. The first cracking load was also verified from the load deflection and load–strain relationships. Table 2 provides a summary of the key experimental results for all beam specimens. The average initial cracking load of series A25 beams is 10.55 kN. The cracking load is directly related to concrete tensile strength which, in turn, is a function of compressive strength, increasing the concrete compressive strength is expected to yield higher cracking loads. The average initial cracking load of the series A45 and A70 beams are 16.25 kN

(a) (b)

Fig. 1. Manufactured GFRP bars. (a) Ribbed 12 mm bars with Crescent shaped lugs (b) double sets of plastic mold.

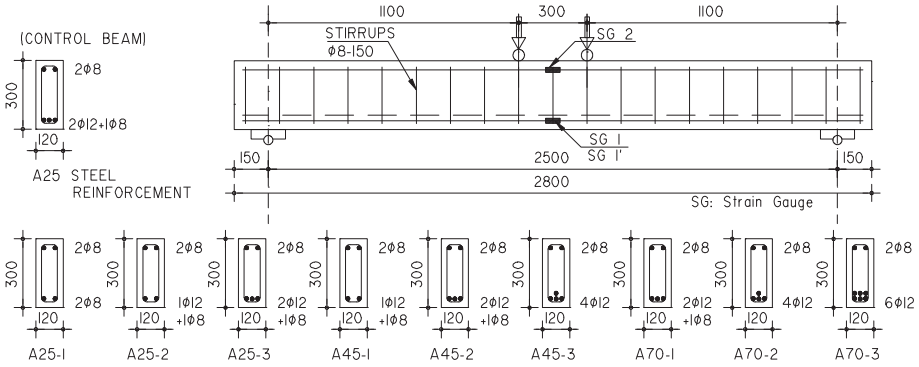

Fig. 2. Tested beams geometry and details.

Table 1
Detail of test beams.

Series	Beam specimen	Beam dimensions		Effective Span, L (mm)	f_{cu} (*MPa*)		Reinforcement ratio[b] (μ) %	Bottom reinforcements (GFRP bars)	Top reinforcements (GFRP bars)	Stirrups (steel)
		Width b(mm)	Depth t (mm)		Target	Actual				
A25	A25[a]	120	300	2500	25	24.5	0.92%	2 φ 12 + 1 φ 8	2 φ 8	8 @ 150
	A25-1	120	300	2500	25	24.5	μ_b	2 φ 8	2 φ 8	8 @ 150
	A25-2	120	300	2500	25	24.5	1.7 μ_b	1 φ 12 + 1 φ 8	2 φ 8	8 @ 150
	A25-3	120	300	2500	25	24.5	2.7 μ_b	2 φ 12 + 1 φ 8	2 φ 8	8 @ 150
A45	A45-1	120	300	2500	45	48	μ_b	1 φ 12 + 1 φ 8	2 φ 8	8 @ 150
	A45-2	120	300	2500	45	48	1.7 μ_b	2 φ 12 + 1 φ 8	2 φ 8	8 @ 150
	A45-3	120	300	2500	45	48	2.7 μ_b	4 φ 12	2 φ 8	8 @ 150
A70	A70-1	120	300	2500	70	74.4	μ_b	2 φ 12 + 1 φ 8	2 φ 8	8 @ 150
	A70-2	120	300	2500	70	74.4	1.7 μ_b	4 φ 12	2 φ 8	8 @ 150
	A70-3	120	300	2500	70	74.4	2.7 μ_b	6 φ 12	2 φ 8	8 @ 150

[a] Steel reinforced beam (control beam).
[b] μ_b was 0.33%, 0.54%, and 0.92% for series A25, A45 and A70 respectively.

Fig. 3. Tested setup and instrumentation.

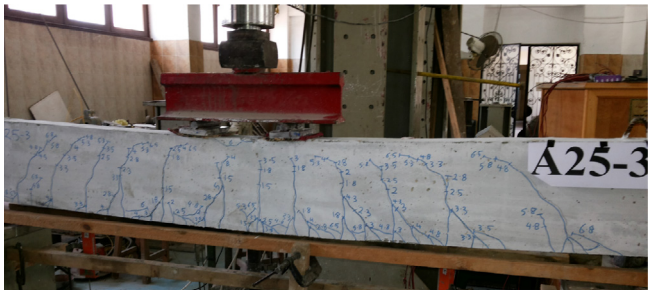

Fig. 4. Crack growth of specimen A25-3.

Table 2
Test results and failure modes.

Series	Beam specimen	Reinforcement Ratio (μ) %	Initial cracking load, P_{ct} (kN)	Failure load, P_{exp} (kN)	Failure modes [a]	Maximum midspan deflection (mm)
A25	A25	0.92%	10.2	74.2	F.F	52
	A25-1	μb	10.2	45.9	G.R	84
	A25-2	1.7 μb	10.8	40.7	G.R	55[b]
	A25-3	2.7 μb	10.9	75.2	C.C	90
A45	A45-1	μb	15.8	55.8	G.R	80
	A45-2	1.7 μb	15.4	81.9	C.C	85
	A45-3	2.7 μb	17.6	109.8	C.C	78
A70	A70-1	μb	16.3	84.6	G.R	88
	A70-2	1.7 μb	15.5	132.7	C.C	95
	A70-3	2.7 μb	19.9	145.1	C.C	92

[a] C.C: concrete crushing, G.R: GFRP bars rupture, F.F: flexure failure due to steel yield.
[b] Sudden rupture of 12 mm diameter GFRP bar.

and 17.23 kN respectively. The ratio of the average cracking load of the series A25 beams to that of the series A70 beams was 1.63. This ratio is close to the ratio between the square root of the average compressive strength of the series A25 beams and that of the series A70 beams, which was 1.73. El-Nemr [9], concluded similar ratios regarding the initial cracking loads for different concrete compressive strength. Although, beam A25-2 exhibited predictable behavior up to about 70% of expected failure load, sudden drop in the load carrying capacity was recorded. It may be due to the local rupture of 12 mm diameter GFRP bar at fixing the strain gauge on the surface of this bar.

3.1. Mode of failure

The failure mechanism for each specimen is given in Table 2. The steel reinforcement control beam, failed in flexure by yielding of the steel bars. Concrete crushing was the most common failure mode, occurring in the specimens of over-reinforced section for glass fiber reinforced specimens. Tension failure in the GFRP reinforcement was characterized by the rupture of GFRP bars at the region of maximum bending moment, it occurs in all beams that are reinforced with GFRP ratio lower than or almost equal the balanced reinforcement ratio μ_b (except for beam A25-2 as discussed earlier). Fig. 5 depicts two sample of concrete crushing and rupture of GFRP failure modes. The non-ductile behavior of GFRP reinforcement makes it suitable for a GFRP member to have compression failure by concrete crushing, which exhibits some warning prior to failure. This requires the GFRP members to be designed for over-reinforcement. El-Nemr [9], recorded the same mode of failure with respect to the balanced reinforcement ratio μ_b.

3.2. Crack patterns

The cracks patterns for series A25 are depicted in Fig. 6, generally, the first cracks were vertical flexural cracks in the vicinity of the tension zone within and near the constant moment region at a load of about 10.55 kN. New cracks continued to form while existing ones propagated vertically toward the compression zone and small branches appear near lower tension surface up to approximately 60% of the maximum load. At higher loading stages, the rate of formation of new cracks significantly decreases. Moreover, the existing cracks grow wider, especially the first formed cracks, and splitting to small short cracks adjacent to the main GFRP bars. It was observed that the cracks located adjacent and/or near the vertical stirrups.

3.3. Crack width

The experimental crack width at the flexural zone was measured by an optical micrometer at sequenced load steps. Fig. 7 reveals that the increasing of reinforcement ratio μ tends to reduce the crack width. At a load of 40 kN, the crack width recorded values of 4.4 mm, 2.7 mm, and 1.2 mm for beam A25-1, A25-1, and A25-3 respectively. While, the crack width is 2.1 mm, 1.15 mm, and 0.70 mm for beam A45-1, A45-2, and A45-3 respectively. In addition, for series A70 the crack width recorded values of 0.90 mm, 0.50 mm, and 0.25 mm for beam A70-1, A70-1, and A70-3 respectively. As shown in Fig. 7(d); specimens with GFRP reinforcement ratio of μ_b, at a load of 40 kN, increasing in the concrete compressive strength from 25 MPa to 45 MPa tends to reduce the crack width by 52%, while the crack width tends to decreased by 80% when the concrete compressive strength increased from 25 MPa to 70 MPa.

Most design codes specify a flexural crack width limit for steel reinforced concrete structures to protect the reinforcing bars from corrosion and to maintain the structure's aesthetic appearance. Unlike steel reinforcement, GFRP is corrosion resistant. The FRP design codes and guidelines permit a larger crack width for FRP-RC elements compared to their counterparts reinforced with steel. CAN/CSA S8063 specified a service-limiting flexural crack width of 0.5 mm for exterior exposure (or aggressive environmental conditions) and 0.7 mm for interior exposure. In addition, ACI 440.1R6 recommends using CAN/CSA S8063 limits for most cases. On the

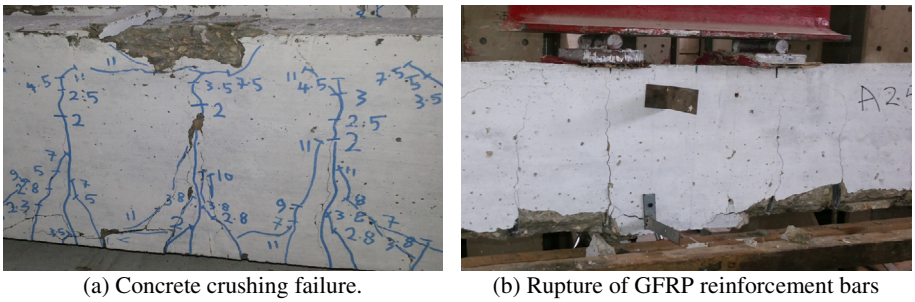

(a) Concrete crushing failure. (b) Rupture of GFRP reinforcement bars

Fig. 5. Modes of failure.

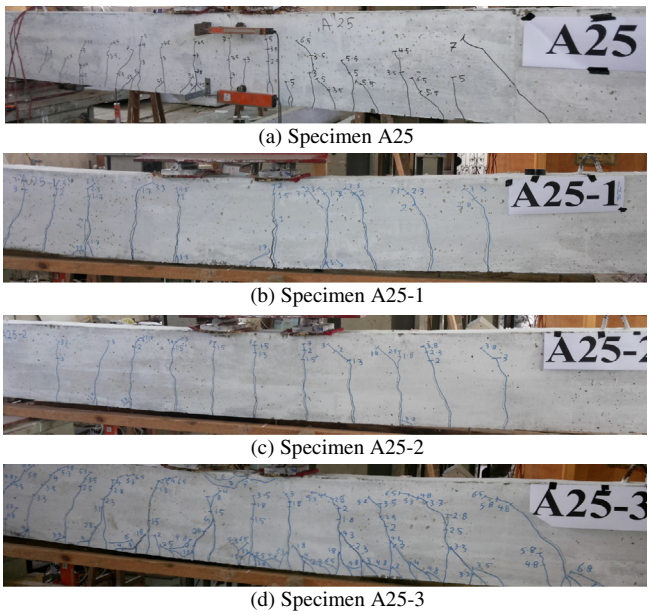

(a) Specimen A25

(b) Specimen A25-1

(c) Specimen A25-2

(d) Specimen A25-3

Fig. 6. Cracks pattern of Series A25 at failure.

other hand, because there is a direct relationship between the strain in the reinforcing bars and the crack width, ISIS14 specified a value of 0.002 as a strain limit in GFRP reinforcing bars to control crack width. At strain value of 0.002, the crack width for beam A25-1, A25-2 and A25-3 is measured 1.1 mm, 0.4 mm and 0.25 respectively. In addition, the crack width is recorded 0.45 mm, 0.3 mm and 0.25 mm for beam A45-1, A45-2 and A45-3 respectively at strain of 0.002. While at same strain value, the measured crack width for beam A70-1, A70-2 and A70-3 is 0.32 mm, 0.15 mm and 0.09 mm respectively.

3.4. Load – deflection behavior

The experimental load to midspan deflection curves and failure loads of the steel and GFRP reinforced concrete beams are presented in Fig. 8 and Table 2. Each curve represents the deflection readings obtained from the LVDT at beam mid-span. The loads to midspan deflection curves were bilinear for all GFRP reinforced beams. The first part of the curve up to cracking represents the behavior of the un-cracked beams. The second part represents the behavior of the cracked beams with reduced stiffness. Nevertheless, GFRP specimens with reinforcement ratio of 2.7 μ_b, can produce some amount of ductility can be provided and overall strength can be compared with control beam.

For the beams in series A25, the GFRP reinforced concrete beams A25-1, A25-2 and A25-3 tend to exhibit greater midspan deflections than control steel reinforcement beam A25. Comparing the midspan deflection of specimens A25-3 and A25, at a given load level, larger deflection in the order of 2.6–4.8 times the deflection of the control specimen A25. This indicates that, for

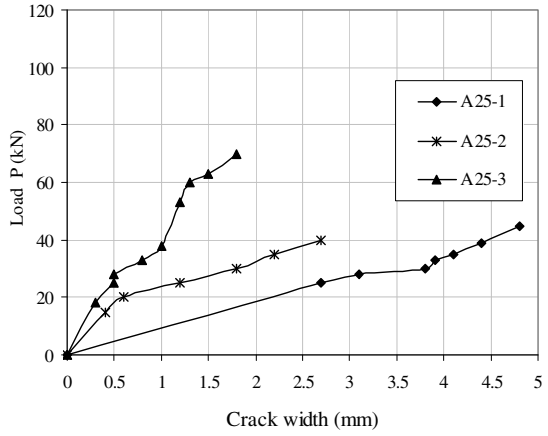

(a) Series A_{25}

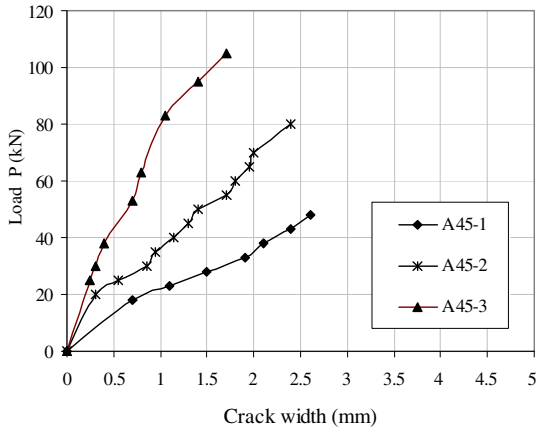

(b) Series A_{45}

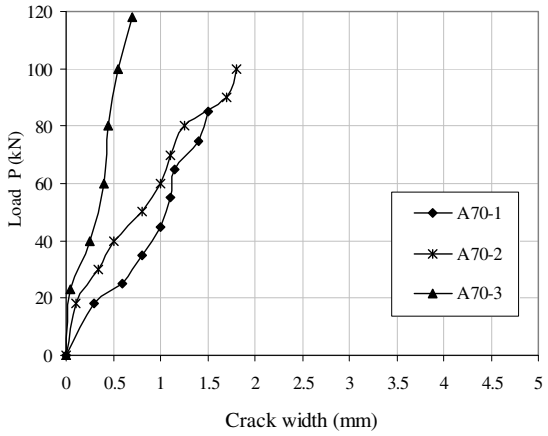

(c) Series A_{70}

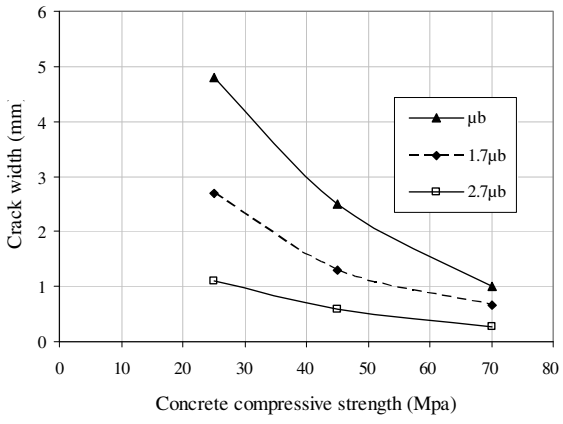

(d) Effect of concrete compressive strength

Fig. 7. Crack width variation with load for different specimens.

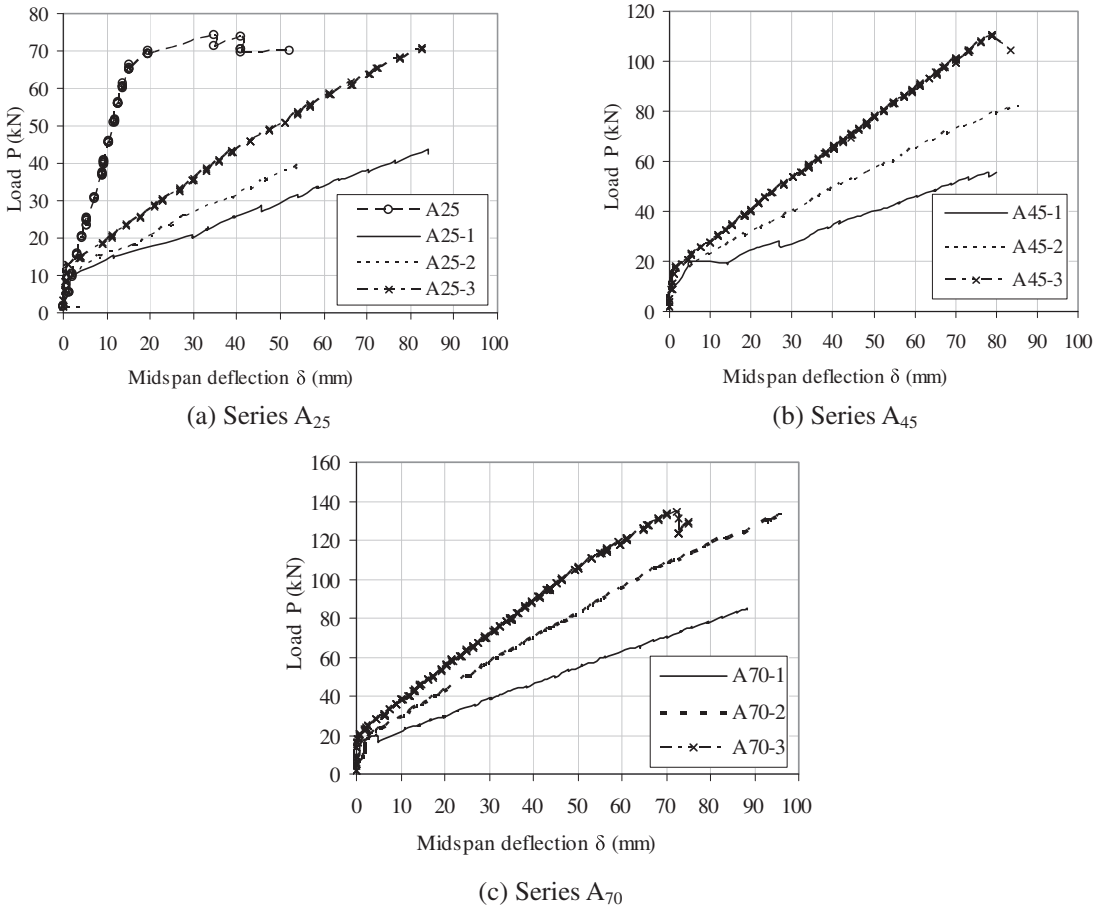

Fig. 8. Load–midspan deflection of tested beams.

the same area of reinforcement, GFRP bars tend to reveal different behavior than steel bars. For GFRP reinforced concrete beams, the midspan deflection tends to decreased as the reinforcement ratio μ increased, similar conclusion has been introduced by Ilker and Ashour [20]. At 20 kN, about twice the cracking load, the midspan deflections were 29.6, 20.3, and 11.2 mm for beams A25-1, A25-2, and A25-3, respectively. Fig. 8(a) could be reveals that increasing the reinforcement ratio from μ_b to 2.7 μ_b, however, increases the ultimate capacity from 45.9 kN to 75.2 kN, giving an increase ratio of 1.63.

Fig. 8(b) shows the load to midspan deflection of series A45. As shown, at the deflection of 80 mm, the ultimate load of specimens A45-2 and A45-3 tends to increased by 47% and 97% with respect to the ultimate load of specimen A45-1 respectively. At 31 kN, about twice the cracking load of series A45, the midspan deflections were 34.5, 18.36, and 12.02 mm for beams A45-, A45-2 and A45-3, respectively.

Fig. 8(c) depicts that increasing the reinforcement ratio from μ_b to 1.7 μ_b, can be increases the ultimate capacity from 84.6 kN to 132.7 kN for beams A70-1 and A70-2, respectively. While increasing the reinforcement ratio from 1.7 μ_b to 2.7 μ_b, however, tends to increases the ultimate capacity from 132.7 kN to 145.1 kN respectively, beam A70-2 and beam A70-3. The midspan deflections at 34 kN, about twice the cracking load, were 26.6, 14.68, and 7.44 mm for beams A70-1, A70-2, and A70-3, respectively.

3.5. Concrete strain at the midspan section

Using the data provided by the two transducers (LVDT) on the concrete surface at the midspan section as shown in Fig. 9, calculation of strains at upper and lower LVDT is carried out. The procedures are summarized in using linear interpolation, applying Bernoulli hypothesis, and then the experimental concrete strain at the extreme compressive fiber is deduced. The neutral axis depth was estimated in the basis of the upper and lower strain calculations for all the tested beams. Fig. 10 shows the concrete strain evolution along the midspan section depth at different load stages for specimens A25-3 and A45-2, respectively.

The maximum compressive strain ε_{cu} was observed to range between 0.29% and 0.66%. These result values are higher than the usual ones established by the American codes of practice [5,4] or the Egyptian codes of practice [18], which consider ε_{cu} to be between 0.3% and 0.35% for the given concrete grades. Abdul Rahman and Narayan [1] obtained compressive strain ε_{cu} of 0.55% for concrete beams reinforced with GFRP bars. According to Cristina and Llinas [17], maximum compressive strain ε_{cu} was observed to be ranged between 0.4% and 0.55%, which agreed with the obtained results.

3.5.1. Neutral axis depth at the midspan section

Taking into account that the cracking loads for the beams depicted in Fig. 11 are 10.4, 16.26, and 17.23 kN for series A25, series A45, and series A70 respectively, it is observed that the neutral axis depth before cracking is located at approximately the mid-height of the section and decreases just after cracking. Afterwards, its value tends to remain constant or decreases slightly, and for high loads it tends to remain constant until the maximum load is achieved showing that concrete is achieving its plastic stage. The neutral axis depth may be increases with the reinforcement ratio, since equilibrium of forces requires a larger

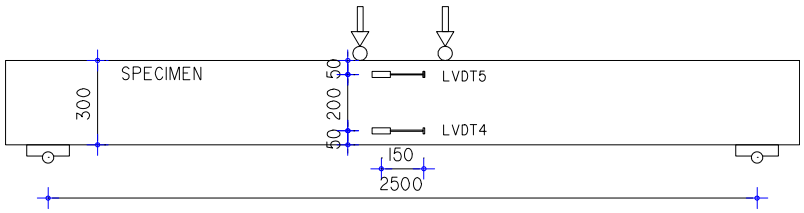

Fig. 9. Position of transducers (LVDT) on concrete at midspan section.

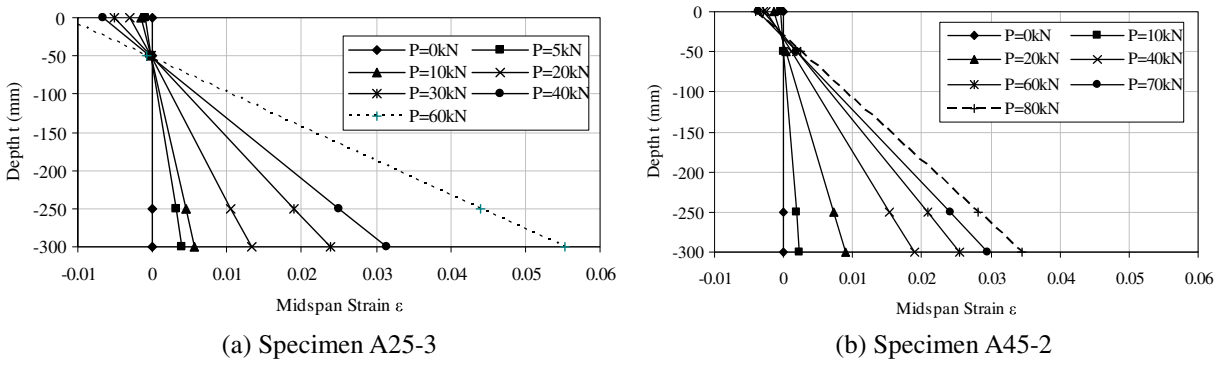

(a) Specimen A25-3 (b) Specimen A45-2

Fig. 10. Concrete strain evolution along the midspan depth.

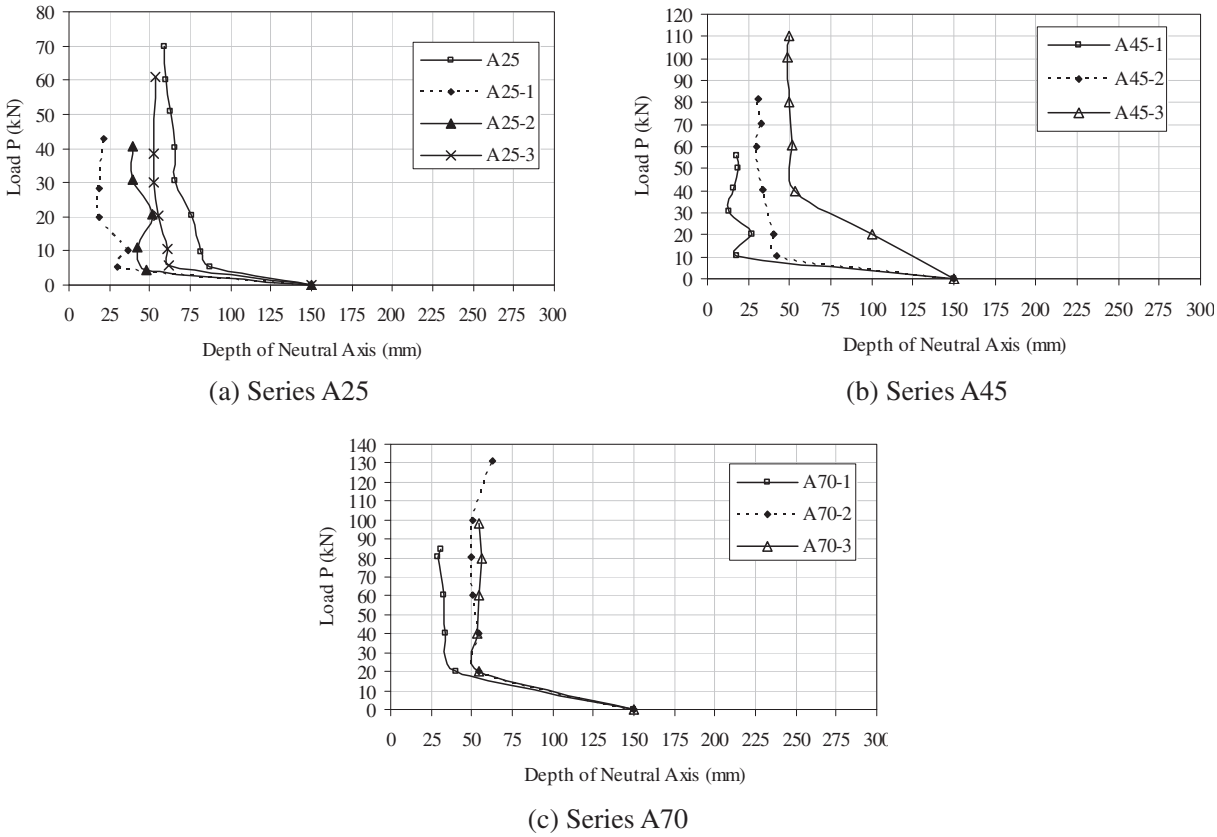

(a) Series A25 (b) Series A45

(c) Series A70

Fig. 11. Estimated neutral axis depth.

compression block for the greater forces arising from larger areas of reinforcement. For the same reinforcement ratio, specimens having higher concrete compressive strength can be possessed higher neutral axis depths. These observations are in agreement with the usual formulation to calculate the neutral axis position in the serviceability conditions in the absence of compression reinforcement.

3.6. Strains in GFRP reinforcement bars

For all specimens, it can be considered a minimal change in the tensile GFRP reinforcement strain until the formation of the first flexural crack. The strain readings of the bottom bar increased rapidly in the vicinity of the first crack load, good agreement with the strain readings and the observation of first cracks was

achieved. The strain distribution in the GFRP reinforcement bars of series A25, A45, and A70 with the load increased is shown in Fig. 12(a)–(c), respectively.

The recorded tensile reinforcement strain for GFRP bars at near failure were in the range of 0.012–0.0177, these strains correspond to about 60–90% of the estimated ultimate strains of the GFRP bars obtained from the tensile test, which reached the value of 0.02. This indicates that rupture of GFRP bars were conducted for high values of tensile strain. However, the low values of tensile strain indicate that the GFRP bars did not rupture at the beam failure. On the other hand, for the control beam, the recorded steel bars strain was about 0.004 at yield and reach 0.0166 at the beam failure.

4. Non-linear finite elements analysis

A non-linear finite element analysis (NLFEA) was conducted to simulate the flexural behavior of concrete beams reinforced with GFRP bars. The commercially available finite element analysis software package, ANSYS (ANSYS release 9.0) [10], was used in this process. The load–deflection curve is considered the key aspect in studying the beams behavior as it involves response parameters including beam ultimate loads, first cracking load, and maximum deflection. Therefore, correlating the load–deflection relationships of the analytical results with that of the experimental ones is considered an effective mean to verify the non-linear model.

The tested beams are symmetric in geometry, loading and internal reinforcement in the longitudinal direction about the mid distance between supports. Only one-half of the beams were modeled by finite element taking advantage of symmetry. Each test beam was typically discretized using 1120 of nearly equal-size 3-D isoparametric elements; Solid65 as shown in Fig. 13(a). The longitudinal reinforcement and transverse shear stirrups are modeled by link 8 element as illustrated in Fig. 13(b).

4.1. NLFEA model verification

The results of NLFEA are compared to the experimental results of the tested beams. For all the beams, flexural cracks appeared when the concrete's tensile strength and, consequently, the cracking moment were reached in the pure bending zone. Cracks were first observed at the tension zone within and near the constant moment region. Under increasing the load, cracks propagated in a vertical direction and further new cracks appeared through the shear span as shown in Fig. 14. Similar findings were recorded by Ibrahim and Salman [8].

Referring to Table 3, the analysis indicated formation of flexural cracks in the test beams at loads of 8.4–11.1 kN, 15.2 kN, and 18.0 kN for specimens with concrete compressive strength of 25 MPa, 45 MPa, and 70 MPa, respectively. The predicted cracking loads; $P_{c\text{-}nu}$ are shown to be in a good agreement with the experimental loads; $P_{c\text{-}exp}$ with a mean $P_{c\text{-}nu}/P_{c\text{-}exp}$ ratio of 0.98 and a coefficient of variation (C.O.V) of 11.2%. A comparison of the predicted with experimental ultimate loads of the test specimens are listed in Table 3. As shown, good agreement between the experimental results and the analysis was achieved. The ratio of the predicted to experimental ultimate strength for the beams ranged between 0.73 and 1.06, with a mean value of 0.88 and a C.O.V of 12.5%. Implicitly, the analysis reflected the significance of test parameters investigated on the load-carrying capacity.

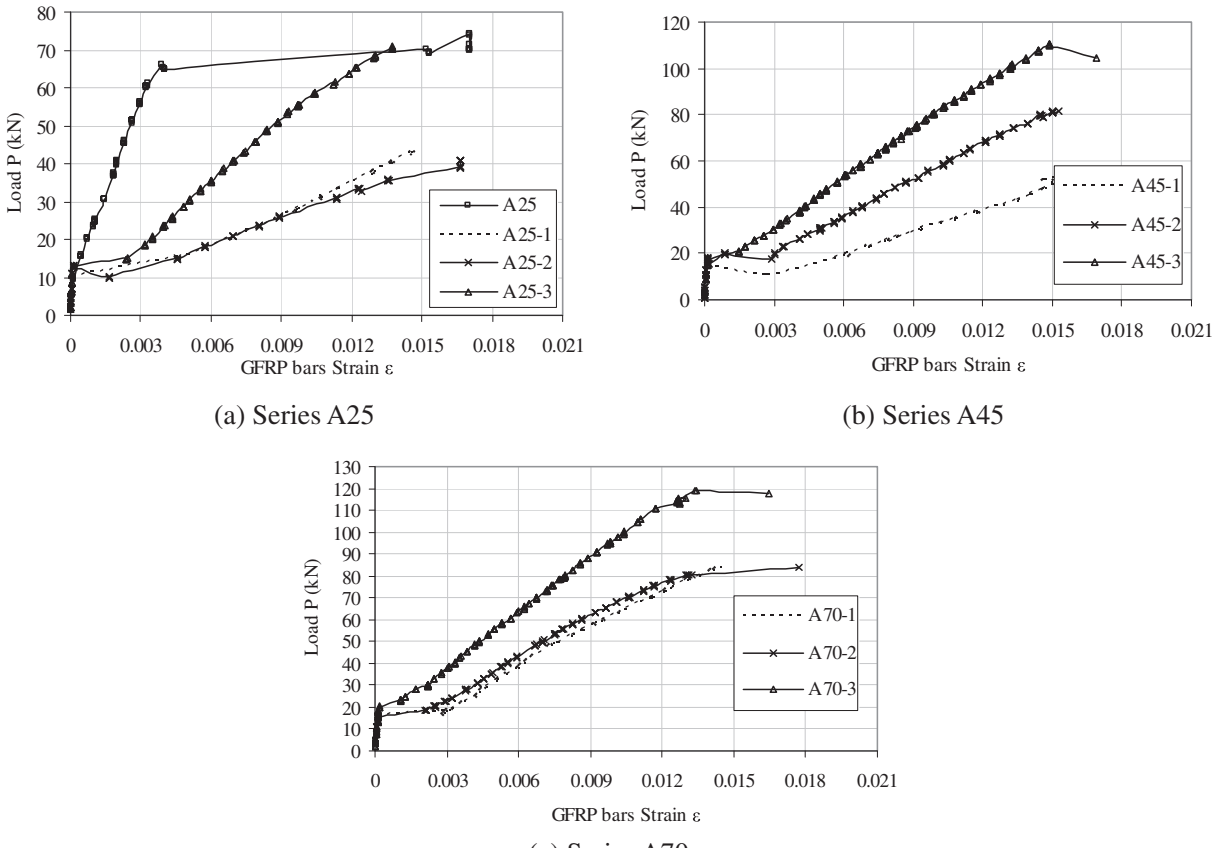

Fig. 12. Load–Strain in the GFRP reinforcement bars.

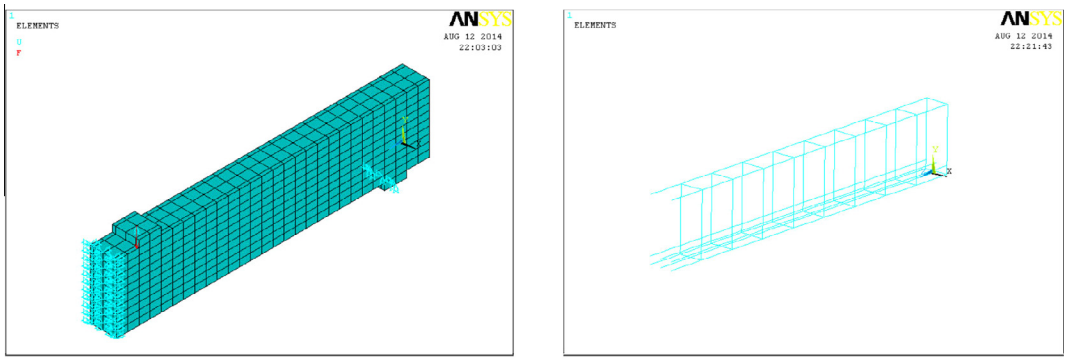

(a) Concrete element; Solid65 (b) Reinforcing bar element; Link8

Fig. 13. Typical idealization of test beam.

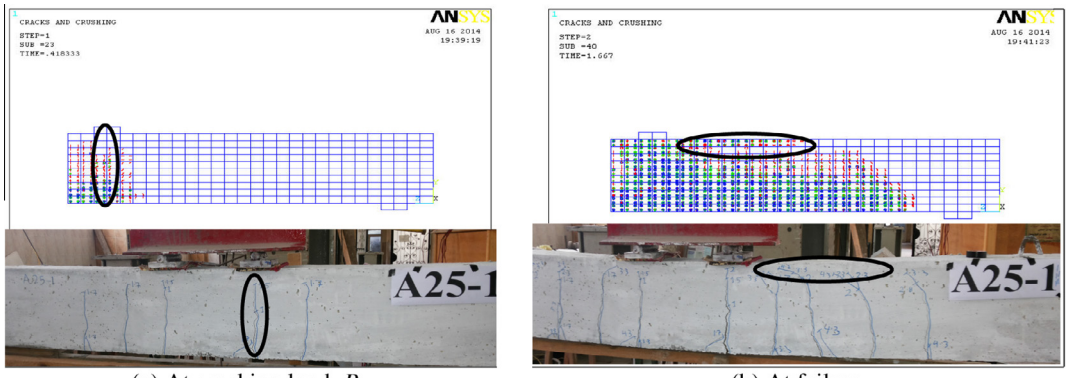

(a) At cracking load, P_{cr} (b) At failure

Fig. 14. Cracks propagation for Specimen A25-1.

Table 3
Comparison of test results with NLFEA results.

Specimens	Experimental results		NLFEA results		Numerical results /Experimental results	
	Cracking load, $P_{ct\text{-}exp}$ (kN)	Failure load, P_{exp} (kN)	Cracking load, $P_{ct\text{-}nu}$ (kN)	Failure load, P_{nu} (kN)	$(P_{ct\text{-}nu})/(P_{ct\text{-}exp})$	$(P_{u\text{-}nu})/(P_{u\text{-}exp})$
A25	10.2	74.2	8.4	75.8	0.82	1.02
A25–1	10.2	45.9	10.5	37	1.02	0.81
A25–2	10.8	40.7	11.0	40[a]	1.02	0.98
A25–3	10.9	75.2	11.1	66.4	1.02	0.88
A45–1	15.8	55.8	15.1	59.4	0.95	1.06
A45–2	15.4	81.9	15.2	75.2	0.98	0.92
A45–3	17.6	109.8	15.2	80	0.86	0.73
A70–1	16.3	84.6	18.2	70	1.11	0.83
A70–2	15.5	132.7	18	100	1.16	0.75
A70–3	19.9	145.1	18	120	0.90	0.83
Mean					0.98	0.88
Standard deviation					0.11	0.11
Coefficient of variation					11.2%	12.5%

[a] Sudden rupture of 12 mm diameter GFRP bar.

5. Analytical models for deflection calculation

5.1. Current deflection approaches brief

Branson's approach represents an expression for an effective moment of inertia (I_e) as follows:

$$I_e = I_g\left(\frac{M_{cr}}{M_a}\right)^3 + I_{cr}\left(1-\left(\frac{M_{cr}}{M_a}\right)^3\right) \leqslant I_g \quad (1)$$

where M_{cr} is the cracking moment; M_a is the service moment. The controlling variable for predicting cracking moment is the modulus of rupture of concrete, f_r. The modulus of rupture used to calculate M_{cr} was taken from the corresponding code or guideline as the following formulas:

$$M_{cr} = \frac{f_r . I_g}{y_b} \text{ where } f_r = 0.6\sqrt{f'_c} \quad (2)$$

Alsayed et al. [7] proposed modification to Branson's approach for the effective moment of inertia based on experimental results. ACI 440.1R-03 [2], Yost and Gross [27], and ECP 208 [18] provided a modified version of Branson's equation that includes a reduction coefficient β_d, which accounts for the bond properties and modulus of elasticity of GFRP bars. ACI 440.1R-06 [4], proposed an

alternative expression for the parameter β_d to account for reduced tension stiffening in FRP-reinforced members, this expression given in Eq. (3).

$$\beta_d = \frac{1}{5}\left(\frac{\rho_f}{\rho_{fb}}\right) \leqslant 1.0 \quad (3)$$

ISIS Canada [21] proposed an expression for the effective moment of inertia based on the assumption that a uniform moment of inertia can be substituted for the actual variable moment of inertia of the beam along its length. Bischoff et al. [14,15] re-evaluated the effective of inertia expression proposed by Branson and incorporated into the ACI Code. Fundamental concepts of tension stiffening were used to propose alternative formulation of effective moment of inertia. Mousavi and Esfahani [22] proposed two models to calculate the effective moment of inertia using the genetic algorithm method.

5.2. Proposed models

Based on the previous equations, there is a need to modify the current ACI equation to predict deflections under service loads. The experimental values of the effective moment of inertia $I_{e\text{-}exp}$ were determined using Eq. (4) as follows:

$$I_{e\text{-}exp} = \frac{P_{exp}L_a}{48E_c\delta_{exp}}(3L^2 - 4L_a^2) \quad (4)$$

A regression analysis was performed on the results for service load range to evaluate the effects of several parameters and to re-evaluate the factor β_d in Branson's equation, Eq. (1). A modification of Branson's equation is proposed so that the predicted values of deflection approach the experimental values. The effects of reinforcement ratio on the factor β_d and in Branson's equation are taken into account. The influence of different parameters is introduced by the coefficients $X1$ and $X2$ in the following Equation:

$$(I_e)_{Theo} = \beta_d\left(\frac{M_{cr}}{M_a}\right)^3 I_g + X2\left[1 - \left(\frac{M_{cr}}{M_a}\right)^3\right] I_{cr} \leqslant I_g \quad (5)$$

where $\beta_d = X1\left(\frac{\rho_f}{\rho_{fb}}\right) \leqslant 1.0$

In order to determine the coefficients $X1$ and $X2$ in Eq. (5), a 3D regression analysis data fit is used to solve nonlinear models with two independent variables; Alsayed et al. [7] used similar analysis for the new proposed model. These data points were obtained from experimental load–displacement relationships of the GFRP reinforced concrete beam specimens. Regression analysis gives us the ability to summarize a collection of sampled data by fitting it to a model that will accurately describe the data. Regression analysis can turn the sampled data points into a smooth continuous function that may be used analytically or utilized by a computer program to return expected values at certain values of the independent variable. The coefficients $X1$ and $X2$ values are 0.227 and 0.60 respectively, the coefficient of multiple determination (R^2) is 0.92 and the standard error fro coefficients $X1$ and $X2$ are 0.005 and 0.009 respectively.

5.3. Evaluation of the proposed model

The values of the effective moment of inertia $(I_e)_{pred}$ determined using the above suggested coefficients, are exploited to predict the mid-span deflection for the tested beam specimens in this study. The serviceability limit considered in this study is taken at a moment of 40% of the failure moment, in other word; the service moment considered in this study is in the range of 1.8–2.8 times the cracking load M_{cr}. On the other hand, deflection at high load

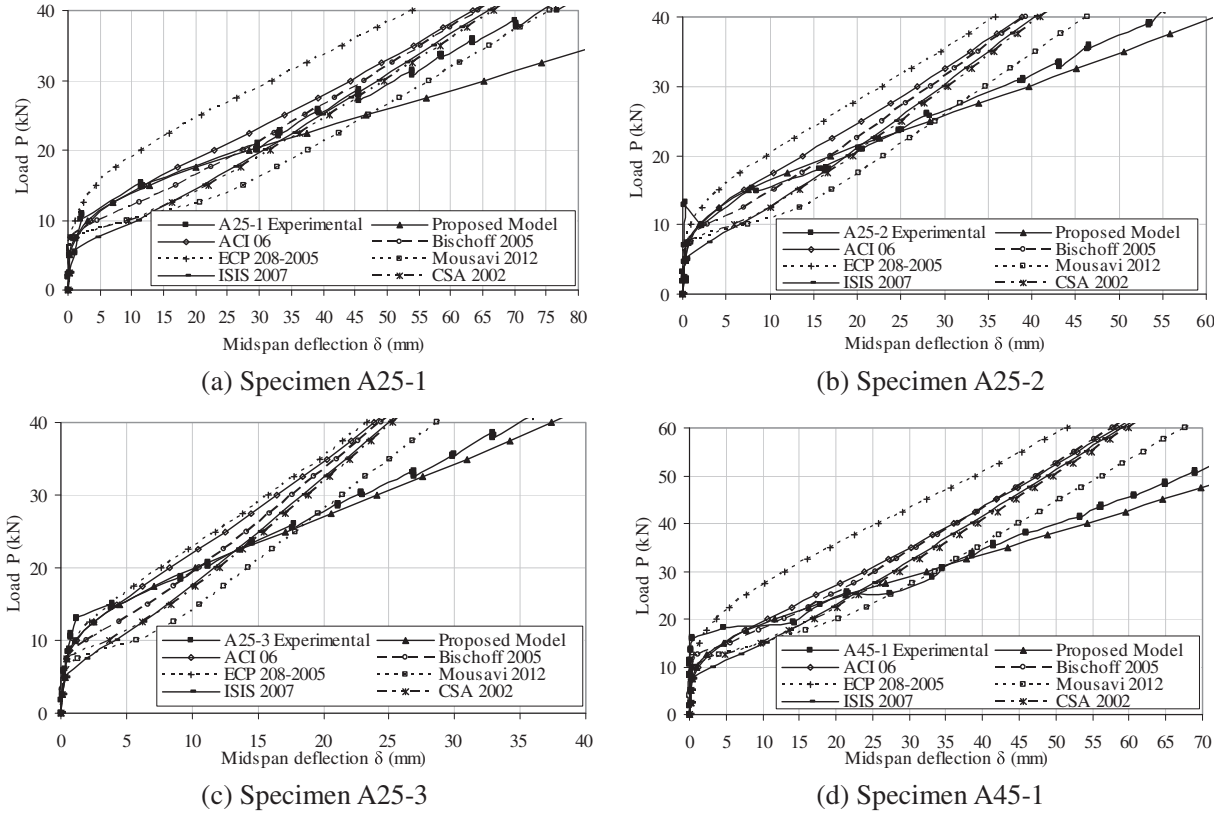

Fig. 15. Comparison of predicted deflections with experimental values.

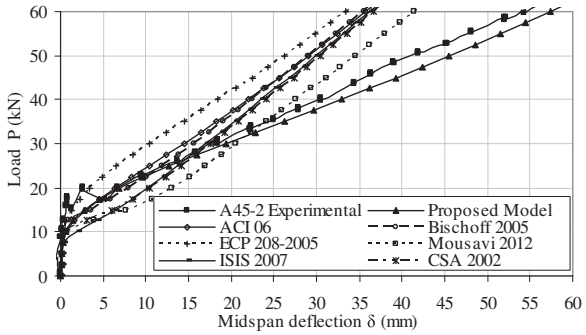

(e) Specimen A45-2

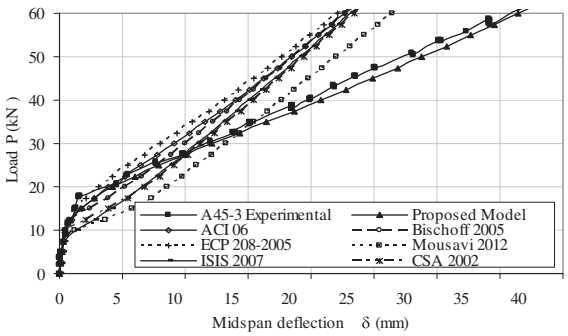

(f) Specimen A45-3

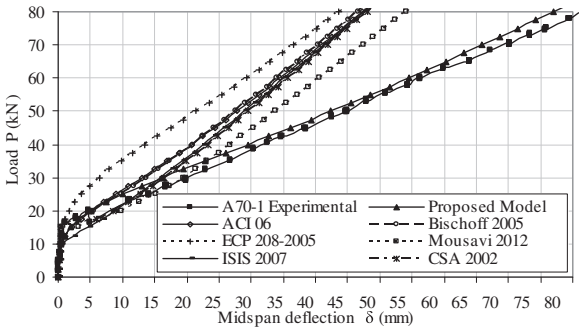

(g) Specimen A70-1

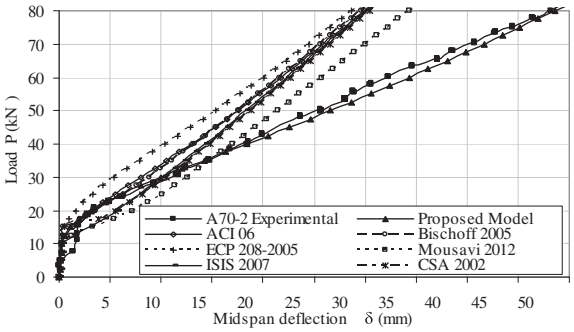

(h) Specimen A70-2

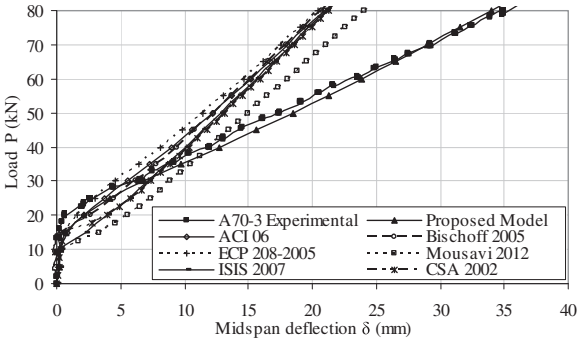

(i) Specimen A70-3

Fig. 15 (*continued*)

limit is discussed in the course of measuring the deflection at four times cracking moment, 4 M_{cr}. A comparison between experimental and predicted load–deflection curves obtained in this study and those predicted by ACI 440.1R [4], ECP 208 [18], ISIS Canada [21], CSA S806-02 [16], Mousavi and Esfahani [22] and Bischoff [14] are presented in Fig. 15(a)–(i), and Table 4.

As depicted in Figs. 15(a)–(i), for all specimens, at serviceability limit state, the proposed model generates a more accurate result as compared with those obtained using the ECP 208 and ACI 440.1R-06 approaches. In general, ECP 208 and ACI 440.1R-06 approaches underestimate deflections particularly for beams with low reinforced ratio. Same findings were reported by Raed Al-Sunna et al. [24] for GFRP reinforced concrete elements with moderate to high reinforced ratio.

The ISIS Canada [21] and CSA S806-02 [16] approaches overestimate deflections (up to 21%) for specimens with low concrete compressive strength and low reinforcement ratio (beams: A25-1, A45-1) at service limit state. However, for specimens with high compressive strength and moderate to high reinforcement ratios (beams: A25-2 to 3, A45-2 to 3 and A70-1 to 3), these approaches underestimate deflection (on average of 81% of experimental deflection). Miàs et al. [28] and Mousavi and Esfahani [22] were recorded overestimation of both ISIS Canada [21] and CSA S806-02 [16] approaches.

At high levels of loading, it is remarkable that the deflections calculated using previous methods are more consistent with each other. The comparisons show that the Mousavi and Esfahani [22], Bischoff [14], ISIS Canada [21] and the CSA S806-02 [16] approaches provide more conservative estimates of deflection than the ECP 208 [18] and ACI 440.1R-06 [4] approaches. This occurs in the methods in which minimum effective moments of inertia, I_e, are equal to the cracked moments of inertia, I_{cr}. The effective moments of inertia at high loading levels and relative high reinforcement ratios are closer to the constant value of I_{cr} using these methods, while experimental effective moments of inertia are less than I_{cr}. An exception that Mousavi and Esfahani [22] approach gives good prediction of effective moments of inertia. The advantage of the current proposed model is its ability to more accurately estimate the effective moment of inertia at values less than that of I_{cr}.

A statistical comparison of the ratio of calculated deflection with experimental value ($\delta_{pred}/\delta_{exp}$) is performed to evaluate the

Table 4
Experimental and predicted deflection.

Beam specimens	Measured deflection (mm)		$\delta_{pred}/\delta_{exp}$ ACI 440.1R [4]		$\delta_{pred}/\delta_{exp}$ ECP 208 [18]		$\delta_{pred}/\delta_{exp}$ ISIS Canada [21]		$\delta_{pred}/\delta_{exp}$ CSA S806 [16]	
	M_{ser}[a]	$\geqslant 4M_{cr}$	M_{ser}[a]	$\geqslant 4M_{cr}$	M_{ser}[a]	$\geqslant 4M_{cr}$	M_{ser}[a]	$\geqslant 4M_{cr}$	M_{ser}[a]	$\geqslant 4M_{cr}$
A25-1	29.7	76.43	0.77	0.83	0.38	0.71	1.03	0.86	1.07	0.88
A25-2	24.85	55.1	0.74	0.70	0.56	0.65	0.91	0.73	0.94	0.74
A25-3	22.6	38.94	0.73	0.68	0.70	0.66	0.81	0.70	0.83	0.71
A45-1	17.9	77.83	0.87	0.69	0.36	0.59	1.16	0.70	1.21	0.71
A45-2	22.2	58.06	0.85	0.64	0.58	0.60	0.86	0.65	0.89	0.65
A45-3	21.86	44.58	0.70	0.61	0.66	0.60	0.74	0.62	0.76	0.62
A70-1	22.8	63.95	0.66	0.59	0.35	0.52	0.77	0.60	0.80	0.61
A70-2	25.7	34.63	0.68	0.67	0.60	0.63	0.71	0.68	0.73	0.70
A70-3	21.71	34.9	0.67	0.60	0.64	0.59	0.69	0.60	0.71	0.61
Mean			0.74	0.67	0.54	0.62	0.86	0.68	0.88	0.69
Standard deviation			0.08	0.07	0.14	0.05	0.16	0.08	0.17	0.08
Coefficient of variation			10.2%%	11.0%	25.3%%	8.7%	18.2%%	12.0%	18.9%	12.1%
Beam specimens	Measured deflection (mm)		$\delta_{pred}/\delta_{exp}$ Mousavi and Esfahani [22]		$\delta_{pred}/\delta_{exp}$ Bischoff [14]		$\delta_{pred}/\delta_{exp}$ NLFEA		$\delta_{pred}/\delta_{exp}$ Proposed model	
	M_{ser}[a]	$\geqslant 4M_{cr}$	M_{ser}[a]	$\geqslant 4M_{cr}$	M_{ser}[a]	$\geqslant 4M_{cr}$	M_{ser}[a]	$\geqslant 4M_{cr}$	M_{ser}[a]	$\geqslant 4M_{cr}$
A25-1	29.7	76.43	1.27	0.99	0.93	0.84	0.82	0.72	0.96	1.31
A25-2	24.85	55.1	1.09	0.84	0.85	0.72	0.74	0.65	0.99	1.11
A25-3	22.6	38.94	0.95	0.80	0.78	0.69	0.80	0.74	1.07	1.08
A45-1	17.9	77.83	1.44	0.81	0.99	0.69	0.89	0.62	1.04	1.10
A45-2	22.2	58.06	1.03	0.74	0.80	0.63	0.73	0.65	1.06	1.03
A45-3	21.86	44.58	0.87	0.70	0.72	0.61	0.76	0.66	1.06	0.99
A70-1	22.8	63.95	0.94	0.69	0.68	0.58	0.68	0.59	0.86	0.95
A70-2	25.7	34.63	0.83	0.79	0.68	0.67	0.70	0.69	1.04	1.07
A70-3	21.71	34.9	0.80	0.69	0.67	0.59	0.77	0.68	1.05	0.97
Mean			1.02	0.78	0.79	0.67	0.77	0.67	1.01	1.07
Standard deviation			0.21	0.10	0.11	0.08	0.07	0.05	0.07	0.11
Coefficient of variation			20.7%%	12.2%%	14.5%%	11.8%	8.7%	7.1%	6.9%	10.0%%

[a] M_{ser} is taken as 40% of failure moment.

accuracy of the proposed and previous approaches of deflection calculation. The average, standard deviation and coefficient of variance for all data, at the serviceability limit state (1.8–2.8 times M_{cr}), and high load level (4.0 M_{cr}) are shown in Table 4. These results show that the deflection prediction developed using the proposed equation, in terms of mean value and standard deviation, is satisfactory. As shown in Table 4, at serviceability limit state, the mean value, standard deviation and C.O.V. of ($\delta_{pred}/\delta_{exp}$) obtained from proposed equation are 1.01%, 0.07% and 6.9% respectively. While at high levels of loading, 4.0 M_{cr}, these values are 1.07%, 0.11% and 10.0% respectively.

The mean and standard deviation values predicted by the ACI 440.1R-06 [4], ECP 208 [18], ISIS Canada [21], CSA S806-02 [16], Mousavi and Esfahani [22] and Bischoff [14] at serviceability limit are 0.74 and 0.08, 0.54 and 0.14, 0.86 and 0.16, 0.88 and 0.17, 1.02 and 0.21, and 0.79 and 0.11 respectively. While at high load level, the mean and standard deviation values predicted by the ACI 440.1R-06 [4], ECP 208 [18], ISIS Canada [21], CSA S806-02 [16], Mousavi and Esfahani [22] and Bischoff [14] are 0.67 and 0.07, 0.62 and 0.05, 0.68 and 0.08, 0.69 and 0.08, 0.78 and 0.1, and 0.67 and 0.08 respectively.

The prediction deflection ($\delta_{pred}/\delta_{exp}$) of NLFEA at serviceability limit and high load limit is also shown in Table 4. The mean value, standard deviation and C.O.V. of ($\delta_{pred}/\delta_{exp}$) obtained from NLFEA are 0.77, 0.07% and 8.7% respectively for serviceability limit. While at high load level, these values are 0.67%, 0.05% and 7.1% respectively.

6. Conclusions

This study investigated the flexural behavior of concrete beams reinforced with locally produced glass fiber reinforced polymer (GFRP) bars. Within the scope of this investigation and considering the materials used, comparison of the experimental results with the values calculated using the proposed equation and other analytical models resulted in the following conclusions:

- The locally produced GFRP bars exhibit reasonable mechanical properties comparing with commercial products in terms of fiber volume fraction (70%), tensile strength (640 MPa), and elastic modulus (30,000 MPa).
- The failure in GFRP RC beams reinforced with more than the balanced reinforcement μb tends to be compression failure due to concrete crushing. While, Beams reinforced with GFRP ratio in order of lower than or almost equal the balanced reinforcement ratio μb shown signs of rupture of GFRP reinforcement.
- Increasing the concrete compressive strength in the order of 25 MPa to 45 MPa tends to reduce in the crack width by 52%, while the crack width tends to decrease by 80% when the concrete compressive strength increased from 25 MPa to 70 MPa.
- The loads deflection curves were bilinear for all GFRP reinforced beams. The first part of the curve up to cracking represents the behavior of the un-cracked beams. The second part represents the behavior of the cracked beams with reduced stiffness. Nevertheless, GFRP specimens with reinforcement ration, 2.7 μb, tend to have some amount of ductility.
- Increasing the reinforcement ratio from μb to 1.7 μb, for series A70, tends to increase the ultimate capacity from 84.6 kN to 132.7 kN respectively. While increasing the reinforcement ratio from 1.7 μb to 2.7 μb, however, tends to increase the ultimate capacity from 132.7 kN to 145.1 kN respectively.
- The maximum concrete compressive strain εcu was recorded between 0.29% and 0.66%.
- The recorded tensile reinforcement strain for GFRP bars reached the range of 0.012–0.0177, these strains correspond to about 60–90% of the estimated ultimate strains of the GFRP bars obtained from the tensile test.

- It can be considered a good agreement between the experimental results and the numerical analysis was achieved in terms of the predicted ultimate loads of the test specimens compared with experimental results. In addition, the numerical analysis reflected the significance of test parameters investigated on the load-carrying capacity.
- ECP 208 and ACI 440.1R-06 approaches tends to underestimate deflections particularly for beams with low reinforced ratio.
- According to the experimental results, the reinforcement ratio and elastic modulus of GFRP bars may be the most significant variables for calculating the deflection. The effects of both aforementioned variables are considered in the equation proposed by Mousavi and Esfahani [22]. The deflection estimated using this model tends to be more accurate than those predicted using many standards and regulations provisions.
- The ECP 208 [18] and ACI 440.1R-06 [4] codes tends to underestimate deflections of concrete beams reinforced with FRP bars. Moreover, deflections calculated using the CSA S806-02 [16] code tends to be more conservative.
- The proposed equation by the current study accounts for the most effective parameters such as modulus of elasticity of FRP bars, relative reinforcement ratio, and levels of loading for calculating the deflection. The influences of the aforementioned parameters were determined through optimization using the regression analysis. The values predicted using the proposed equation correlate well with the experimental values.
- The proposed equation can better predict deflection when effective moment of inertia is less than Icr, especially at high levels of loading and reinforcement ratios.

Acknowledgments

The authors wish to acknowledge the financial support of the Civil Engineering Department, Faculty of Engineering Shoubra, Benha University, Cairo, Egypt. The first author is grateful of the chemical company BASF for supplied a free charge concrete admixtures.

References

[1] Abdul Rahman MS, Narayan SR. Flexural behaviour of concrete beams reinforced with glass fibre reinforced polymer bars. J Kejuruteraan Awam 2005;17(1):49–57.
[2] ACI Committee 440. ACI 440.1R-03, Guide for the design and construction of concrete reinforced with FRP bars. Farmington Hills, Mich., USA: American Concrete Institute (ACI); 2003.
[3] ACI Committee 440. ACI 440.3R-04, Guide test methods for fiber-reinforced polymers (FRPs) for reinforcing or strengthening concrete structures. Farmington Hills, Mich., USA: American Concrete Institute (ACI); 2004.
[4] ACI Committee 440. ACI 440.1R-06, Guide for the design and construction of concrete reinforced with FRP bars. Farmington Hills, Mich., USA: American Concrete Institute (ACI); 2006.
[5] ACI Committee 318. ACI 318R-05. Building code requirements for structural concrete (ACI 318-11) and commentary (ACI 318R-11). Farmington Hills, Mich., USA: American Concrete Institute (ACI); 2011.
[6] Shanour Ali S. Behavior of concrete beams reinforced with GFRP bars [Ph.D. dissertation], Faculty of Engineering, Shoubra, Benha University, Cairo, Egypt; due 2014.
[7] Alsayed SH, Al-Salloum YA, Almusallam TH. Performance of glass fiber reinforced plastic bars as a reinforcing material for concrete structures. Comp Part B Eng 2000;31(6–7):555–67.
[8] Ibrahim Amer M, Salman WD. Finite element analysis of reinforced concrete beams strengthened with CFRP in flexural. Diyala J Eng Sci 2009;02(02):88–104.
[9] El-Nemr Amr, Ahmed Ehab A, Benmokrane B. Flexural behavior and serviceability of normal- and high-strength concrete beams reinforced with glass fiber-reinforced polymer bars. ACI Struct J 2013;110(6).
[10] ANSYS®. Engineering analysis system user's manual. Theoretical manual, revision 8.0, vol. 1, 2. Houston, Pennsylvania: Swanson Analysis System Inc.; 2004.
[11] ASTM, Designation: D 2584–02. Standard test method for ignition loss of cured reinforced resins; 2002.
[12] Balendran RV, Tang WE, Leung HY, Nadeem A. Flexural behaviour of sand coated glass-fiber reinforced polymer (GFRP) bars in concrete. In: 29th conference on our world in concrete & structures. Singapore; 2004.
[13] Benmokrane B, Chaallal O, Masmoudi R. Flexural response of concrete beams reinforced with FRP reinforcing bars. ACI Struct J 1996;91(2):46–55.
[14] Bischoff PH. Reevaluation of deflection prediction for concrete beams reinforced with steel and fiber reinforced polymer bars. ASCE J Struct Eng 2005;131(5):752–62.
[15] Bischoff PH, Scanlon A. Effective moment of inertia for calculating deflections of concrete members containing steel reinforcement and FRP reinforcement. ACI Struct J 2007;104(1):68–75.
[16] CAN, CSA S806-02. Design and construction of building components with fibre reinforced polymers. Rexdale, Ontario, Canada: Canadian Standards Association; 2002. 177 pp.
[17] Cristina Barris P, Lluis Torres Llinas. Serviceability behaviour of fibre reinforced polymer reinforced concrete beams [Ph.D. thesis]. Girona, Catalonia, Spain: University of Girona; 2010.
[18] ECP 208. Egyptian code of practice for design principles of the use of fiber reinforced polymers in construction. Permanent committee, Code No. 208. Cairo, Egypt; 2005.
[19] El-Salakawy E, Chakib Kassem, Brahim Benmokrane. Flexural behaviour of concrete beams reinforced with carbon FRP composite bars. In: 4th structural specialty conference of the canadian society for civil engineering montréal. Québec, Canada; June 5–8, 2002.
[20] Kara Ilker Fatih, Ashour Ashraf F. Flexural performance of FRP reinforced concrete beams. J Comp Struct 2012;29 [Available Online 29 December 2011].
[21] ISIS Canada. Reinforced concrete structures with fibre reinforced polymers – design manual No. 3. Manitoba, Canada: ISIS Canada Corporation, University of Manitoba; 2007. 158 pp.
[22] Mousavi S Roohollah, Esfahani M Reza. Effective moment of inertia prediction of FRP-reinforced concrete beams based on experimental results. ASCE J Comp Constr 2012;16(5):490–8.
[23] Nanni A. North American design guidelines for concrete reinforcement and strengthening using FRP: principles, applications and unresolved issues. Constr Build Mater 2003;17:439–46.
[24] Al-Sunna Raed, Pilakoutas K, Hajirasouliha I, Guadagnini M. Deflection behaviour of FRP reinforced concrete beams and slabs: an experimental investigation. Compos Part B Eng 2012;43(5):2125–34 [Online publication date: 1-Jul-2012].
[25] Raffaello F, Andrea P, Domenico A. Limit states design of concrete structures reinforced with FRP bars [Ph.D. thesis]. Naples, Italy: University of Naples Federico.
[26] Pecce M, Manfredi G, Cosenza E. Experimental response and code models of GFRP RC beams in bending. ASCE J Comp Constr 2000;4(4):182–90.
[27] Yost JR, Gross SP, Dinehart DW. Effective moment of inertia for glass fiber-reinforced polymer-reinforced concrete beams. ACI Struct J 2003;100(6):732–9.
[28] Miàs C, Torres L, Turon A, Barris C. Experimental study of immediate and time-dependent deflections of GFRP reinforced concrete beams. Compos Struct 2013;96(2013):279–85.